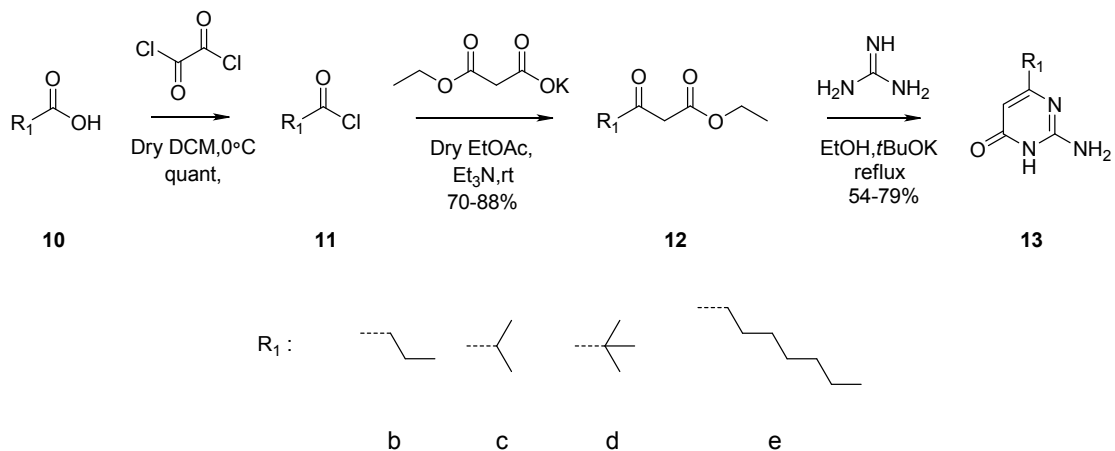
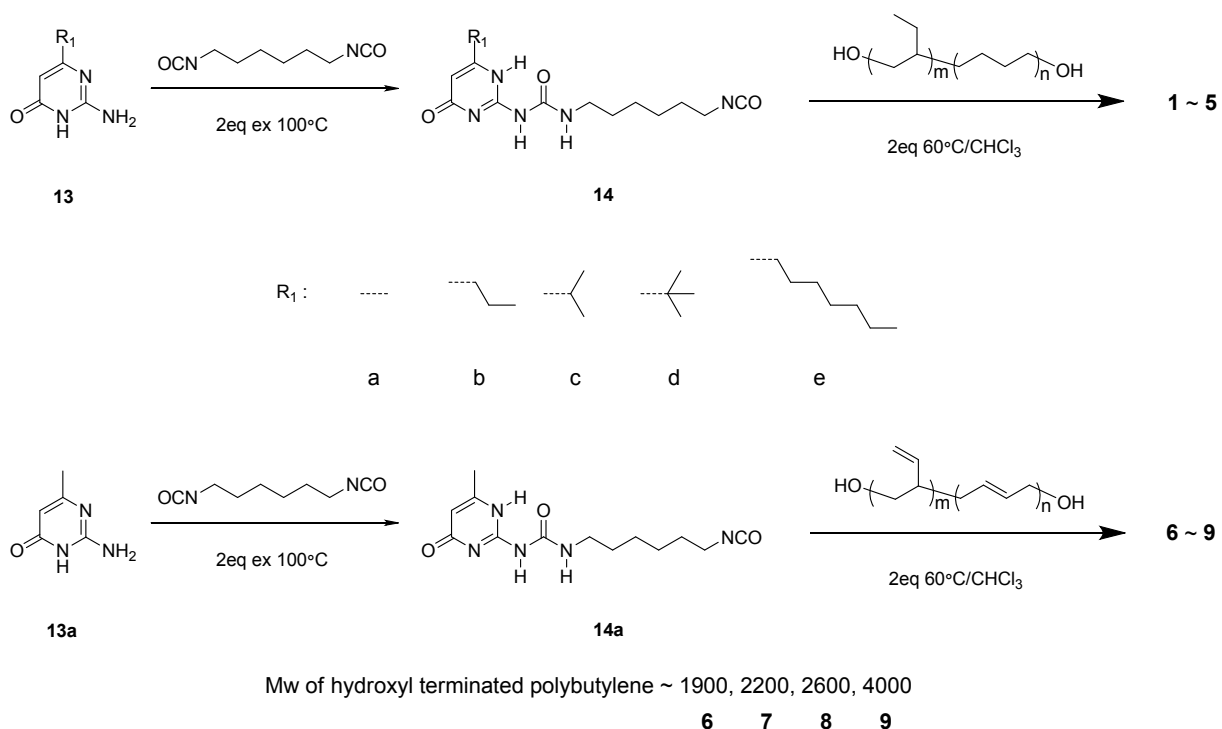


Supporting information

Experimental procedure:



Scheme S1. Synthesis route towards isocytosines **13a** ~**13e**.



Scheme S2. Synthesis route towards polymers **1** ~ **9**.

Butyryl chloride (11b)

Butyric acid 10b (8.8 g, 100 mmol) was dissolved in dry dichloromethane (200 mL) and cooled on an ice bath. A solution of oxalylchloride (10.2 mL, 120 mmol, 1.2 eq) in dry dichloromethane (100 mL) was added dropwise and stirred for an additional 15 min under an argon atmosphere. The solution was stirred at room temperature for 4 h, after which the solution was evaporated *in vacuo* to yield the product as a yellow oil.

Isobutyryl chloride (11c)

The synthesis was performed as described for 8a. The product was evaporated in vacuo.

Pivaloyl chloride (11d)

The synthesis was performed as described for 8a. The product was evaporated in vacuo.

Octanoyl chloride (11e)

The synthesis was performed as described for 8a. The product was evaporated in vacuo.

Ethyl 3-oxohexanoate (12b)

Potassium ethyl malonate (10.30 g, 60.5 mmol, 1.4 eq) was dissolved in dry ethyl acetate (200 mL) under an argon atmosphere. The mixture was cooled on an ice bath and anhydrous magnesium chloride (6.89g, 72.5 mmol, 1.7 eq) and dry triethylamine (21 mL, 150.6 mmol, 3.5 eq) were added. The mixture was stirred at 35°C under an argon atmosphere for 6 h, after which the mixture was cooled on an ice bath. A solution of butyryl chloride 11b (4.97 g, 46.9 mmol) in dry ethyl acetate (50 mL) was added dropwise and the mixture was stirred at room temperature under an argon atmosphere overnight. The mixture was cooled on an ice bath and 200 mL 13% HCl was added dropwise. The aqueous layers were separated and extracted with chloroform:ethyl acetate (1:1 v/v, 100 mL) and the combined organic layer was extracted with 13% HCl (2x100 mL), H₂O (100 mL), brine (100 mL), 5 wt% KHCO₃ (3x100 mL), brine (100 mL), dried over MgSO₄ and evaporated *in vacuo* to yield the product as a yellow oil.

¹H NMR (500 MHz, CDCl₃): δ 12.06, 4.93, 4.14, 3.39, 2.50, 1.54, 1.23, 0.86

Ethyl 4-methyl-3-oxopentanoate (12c)

The synthesis and purification were performed as described for 12b. The product was obtained as a yellow oil.

¹H NMR (500 MHz, CDCl₃): δ 12.13, 4.95, 4.18, 3.47, 2.71, 1.26, 1.12

Ethyl 4,4-dimethyl-3-oxopentanoate (12d)

The synthesis and purification were performed as described for 12b. The product was obtained as a yellow oil.

¹H NMR (500 MHz, CDCl₃): δ 12.32, 5.02, 4.16, 3.52, 1.25, 1.15

Ethyl 3-oxodecanoate (12e)

The synthesis and purification were performed as described for 12b. The product was obtained as a yellow oil.

^1H NMR (500 MHz, CDCl_3): δ 12.08, 4.95, 4.18, 3.41, 2.51, 1.26, 0.85

2-amino-6-propylpyrimidin-4(1H)-one (13b)

Ethyl 3-oxohexanoate 12b (6.24 g, 39.5 mmol), guanidine carbonate (5.21 g, 57.9 mmol, 1.3 eq) and potassium tert-butoxide (4.55 g, 40.5 mmol, 1 eq) were dissolved in ethanol (140 mL) and stirred at reflux for 3 days. The solvent was removed in vacuo and the citric acid aqueous solution was added and the pH was adjusted about 5. The precipitate was filtered and washed with diluted citric acid aqueous solution and deionized water until the pH of the filtrate was about 7. The precipitate was collected and dried *in vacuo* to get the pale-yellow powder.

FT-IR ν (cm^{-1}) = 3336, 3091, 2967, 2936, 2876, 1662, 1641, 1620, 1554, 1464, 1400.

2-amino-6-isopropylpyrimidin-4(1H)-one (13c)

The synthesis and purification were performed as described for 13b. The product was obtained as a pale-yellow powder.

FT-IR ν (cm^{-1}) = 3339, 3080, 2968, 1664, 1494, 1385, 1321, 838, 774.

2-amino-6-(tert-butyl)pyrimidin-4(1H)-one (13d)

The synthesis and purification were performed as described for 13b. The product was obtained as a pale-yellow powder.

FT-IR ν (cm^{-1}) = 3357, 3093, 2964, 1660, 1511, 1403, 1378, 1360, 838, 772.

2-amino-6-heptylpyrimidin-4(1H)-one (13e)

The synthesis and purification were performed as described for 13b. The product was obtained as a pale-yellow powder.

FT-IR ν (cm^{-1}) = 3326, 3077, 2956, 1666, 1501, 1376, 1360, 554.

1-(6-isocyanatohexyl)-3-(6-methyl-4-oxo-1,4-dihydropyrimidin-2-yl)urea (14a)

A solution of 87.5 g (0.70 mol) 2-amino-4-hydroxy-6-methylpyrimidine in 798 g (4.75 mol) hexyldiisocyanate was heated at 100°C for 16 h. After cooling down to room temperature, 2 liters hexane was added and the resulting precipitate was filtered and washed with pentane. The white powder was dried at 50°C under vacuum. The excess of hexyldiisocyanate was recovered by distillation.

^1H NMR (500 MHz, CDCl_3): δ 13.1, 11.9, 10.2, 5.8, 3.3, 2.2, 1.6, 1.4.

FT-IR ν (cm^{-1}) = 3033, 2933, 2856, 2283, 1701, 1667, 1579, 1524, 1255.

1-(6-isocyanatohexyl)-3-(4-oxo-6-propyl-1,4-dihydropyrimidin-2-yl)urea (14b)

A solution of 3.06 g (20 mmol) 2-amino-6-propylpyrimidin-4(1H)-one in 33.6 g (0.2 mol) hexyldiisocyanate was heated at 90°C for 48 h to obtain a pale-yellow solution. After cooling down to -25°C for 48 h, white crystal separated out and 100 mL -25°C hexane was added and the resulting precipitate was filtered and washed with cold

hexane. The white powder was dried at 50°C under vacuum. The product was obtained as a pale-yellow powder. The excess of hexyldiisocyanate was recovered by distillation.

¹H NMR (500 MHz, CDCl₃): δ 13.2, 11.9, 10.2, 5.8, 3.3, 2.5, 1.7, 1.6, 1.4, 1.3, 1.0.

FT-IR ν (cm⁻¹) = 2957, 2934, 2859, 2290, 1701, 1658, 1591, 1530, 1462, 1312, 1260, 793, 743.

1-(6-isocyanatohexyl)-3-(6-isopropyl-4-oxo-1,4-dihydropyrimidin-2-yl)urea (14c)

The synthesis and purification were performed as described for 14b. The product was obtained as a pale-yellow powder.

¹H NMR (500 MHz, CDCl₃): δ 13.3, 11.9, 10.2, 5.9, 3.3, 2.7, 1.6, 1.4, 1.3.

FT-IR ν (cm⁻¹) = 2970, 2942, 2876, 2302, 1705, 1649, 1571, 1462, 1264, 1243.

1-(6-(*tert*-butyl)-4-oxo-1,4-dihydropyrimidin-2-yl)-3-(6-isocyanatohexyl)urea (14d)

The synthesis and purification were performed as described for 14b. The product was obtained as a pale-yellow powder.

¹H NMR (500 MHz, CDCl₃): δ 13.5, 12.0, 10.2, 5.9, 3.3, 1.6, 1.4, 1.3.

FT-IR ν (cm⁻¹) = 2942, 2278, 1702, 1640, 1572, 1526, 1264, 1245.

1-(6-heptyl-4-oxo-1,4-dihydropyrimidin-2-yl)-3-(6-isocyanatohexyl)urea (14e)

The synthesis and purification were performed as described for 14b. The product was obtained as a pale-yellow powder.

¹H NMR (500 MHz, CDCl₃): δ 13.2, 11.9, 10.2, 5.8, 3.3, 2.4, 2.3, 1.6, 1.4, 1.3, 1.0, 0.9.

FT-IR ν (cm⁻¹) = 3225, 3137, 3028, 2941, 2862, 2267, 1663, 1614, 1560, 1457, 1393, 1325.

***O,O'*-Bis-{6-(4[1*H*]-oxo-pyrimidinyl-6-methyl-2-ureido)hexylcarbamate}-hydrogenated polybutadiene (1)**

Hydroxyl-terminated polybutadiene (35 g, 10 mmol) and 1-(6-isocyanatohexyl)-3-(6-methyl-4-oxo-1,4-dihydropyrimidin-2-yl)urea (6.45 g, 22 mmol) and 1 drop of dibutyltin dilaureate were stirred in dry chloroform (500 mL) under an argon atmosphere at 60°C for 24 h. Silica and dibutyltin dilaureate (few drops) were added and stirred at reflux under an argon atmosphere for 24 h. The mixture was cooled to room temperature, filtered, concentrated in vacuo and the residue precipitated in acetone to yield the product as a colorless solid.

¹H NMR (500 MHz, CDCl₃): δ 13.1, 11.9, 10.1, 5.9, 4.1, 3.2, 2.2, 2.0, 1.5 ~ 0.8.

FT-IR ν (cm⁻¹) = 2959, 2925, 2855, 1700, 1664, 1590, 1526, 1462, 1379, 1253.

***O,O'*-Bis-{6-(4[1*H*]-oxo-pyrimidinyl-6-propyl-2-ureido)hexylcarbamate}-hydrogenated polybutadiene (2)**

The synthesis and purification were performed as described for **5**. The products were obtained as colorless solids.

$^1\text{H NMR}$ (500 MHz, CDCl_3): δ 13.3, 11.9, 10.1, 5.9, 4.1, 3.5, 1.6, 1.3, 0.8.

FT-IR ν (cm^{-1}) = 2960, 2925, 2855, 1700, 1661, 1589, 1526, 1462, 1379, 1253.

***O,O'*-Bis-{6-(4[1*H*]-oxo-pyrimidinyl-6-isopropyl-2-ureido)hexylcarbamate}-hydrogenated polybutadiene (3)**

The synthesis and purification were performed as described for **5**. The products were obtained as colorless solids.

$^1\text{H NMR}$ (500 MHz, CDCl_3): δ 13.3, 11.9, 10.2, 5.9, 4.1, 3.2, 2.2, 2.0, 1.6, 1.3, 0.8.

FT-IR ν (cm^{-1}) = 2960, 2925, 2854, 1699, 1660, 1588, 1528, 1462, 1379, 1257.

***O,O'*-Bis-{6-(4[1*H*]-oxo-pyrimidinyl-6-heptyl-2-ureido)hexylcarbamate}-hydrogenated polybutadiene (4)**

The synthesis and purification were performed as described for **5**. The products were obtained as colorless solids.

$^1\text{H NMR}$ (500 MHz, CDCl_3): δ 13.5, 12.0, 10.2, 5.9, 4.1, 3.2, 1.6, 1.3, 0.8.

FT-IR ν (cm^{-1}) = 2960, 2925, 2855, 1699, 1656, 1585, 1528, 1462, 1379, 1250.

***O,O'*-Bis-{6-(4[1*H*]-oxo-pyrimidinyl-6-*tert*-butyl-2-ureido)hexylcarbamate}-hydrogenated polybutadiene (5)**

The synthesis and purification were performed as described for **5**. The products were obtained as colorless solids.

$^1\text{H NMR}$ (500 MHz, CDCl_3): δ 13.2, 11.9, 10.1, 5.9, 4.1, 3.2, 1.6, 1.3, 0.8.

FT-IR ν (cm^{-1}) = 2960, 2925, 2855, 1699, 1660, 1588, 1526, 1462, 1379, 1252.

***O,O'*-Bis-{6-(4[1*H*]-oxo-pyrimidinyl-6-methyl-2-ureido)hexylcarbamate}-polybutylene (6)**

Hydroxyl-terminated polybutadiene (19 g, 10 mmol) and 1-(6-isocyanatohexyl)-3-(6-methyl-4-oxo-1,4-dihydropyrimidin-2-yl)urea (6.45 g, 22 mmol) and 1 drop of dibutyltin dilaureate were stirred in dry chloroform (500 mL) under an argon atmosphere at 60°C for 24 h. Silica and dibutyltin dilaureate (few drops) were added and stirred at reflux under an argon atmosphere for 24 h. The mixture was cooled to room temperature, filtered, concentrated in vacuo and the residue precipitated in acetone to yield the product as a colorless solid.

$^1\text{H NMR}$ (500 MHz, CDCl_3): δ 13.1, 11.9, 10.1, 5.4, 4.9, 3.2, 2.2, 2.0, 1.6, 1.3.

FT-IR ν (cm^{-1}) = 2918, 2846, 1699, 1667, 1587, 1526, 1440, 1257, 966, 911.

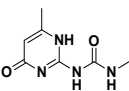
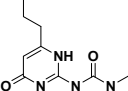
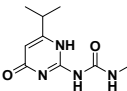
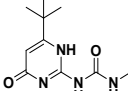
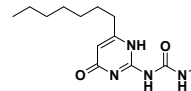
Poymer 7 ~ 9

The synthesis and purification were performed as described for **6**. The products were obtained as colorless solids.

Table S1 Molecular weight and thermal properties of supramolecular polymers **1** ~ **5**.

Polymer	M_n ($\text{g}\cdot\text{mol}^{-1}$)	T_g ($^{\circ}\text{C}$)	T_m ($^{\circ}\text{C}$)	melting enthalpy ($\text{J}\cdot\text{g}^{-1}$)	peak area ($\text{MPa}\cdot\text{min}$)
1	4086	-44.6	65.6	7.8	853
2	4142	-47.3	62.8	6.1	800
3	4142	-47.4	53.1	0.42	625
4	4170	-47.1	52.6	0.149	619
5	4254	-46.8	52.2	0.05	614

Table S2 The total energy of the different chemical structures of the ureido-pyrimidone.
(ChemBio3D Ultra 12.0, MM2 Minimize)

Structure					
Steric energy	1.032	2.551	3.496	4.541	6.686
$\text{kcal}\cdot\text{mol}^{-1}$					

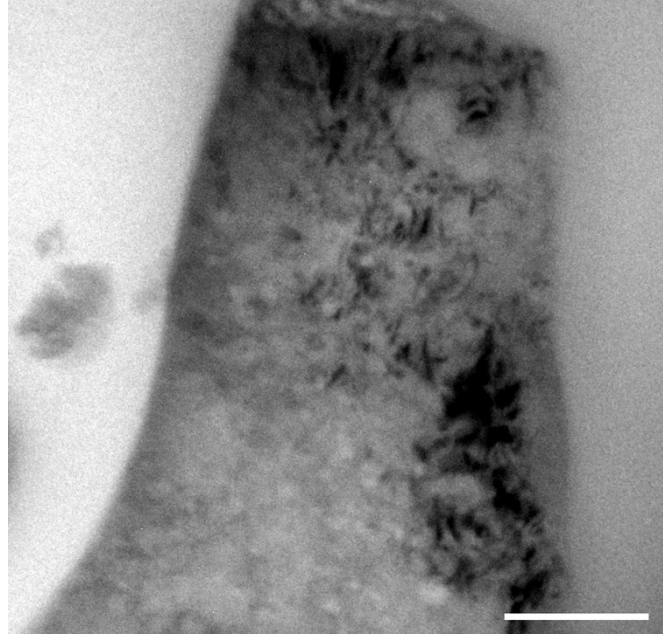


Figure S1 The TEM image of polymer **1**. Scale bar, 200 nm.

Figure S1 showed the TEM image of the polymer **1**. Because of the polymer was organic compounds, and the difference between the density of the nanofiber to the telechelic PEB was not too much, the contrast between the two phases was hard to be distinguished. Moreover, the polymer film was too thin to afford the electron beam so that it was dyed by osmium tetroxide solution to enhance the contrast in order to get an ideal image. The dark motif in the TEM image was the nanofibers dyed after the osmium tetroxide solution and the diameter of them match the data with AFM image about 10 nm.

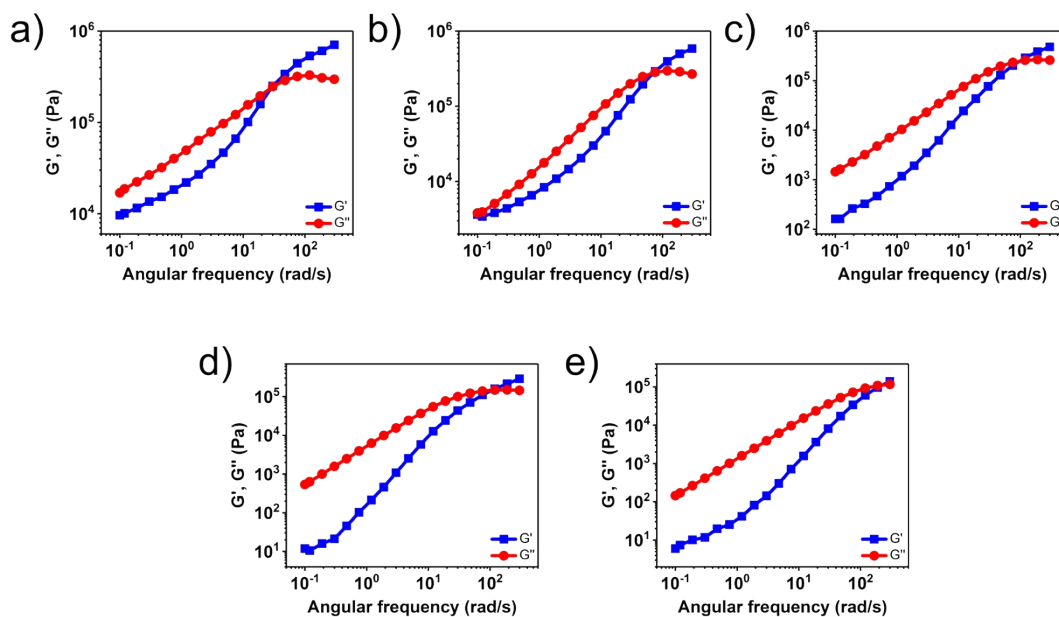


Figure S2 The rheology tests of sample **1** to **5** from a to e.

As shown in figure S2, the ratios of the slope of G' to G'' of polymer **1** and polymer **2** were about 1:1, indicating that there were significant interactions between supramolecular polymer and small clusters of hydrogen-bonded units were existed in the solid. These clusters act as hard domains and physical crosslinks in supramolecular polymers, which corresponding to the nano-fibers structures in the solid. With the steric hindrance of the six-position increased, the ratio of the slope of G' to G'' gradually changed to 1:2, indicating that the cluster in the solid disappeared and the interaction between the UPy dimmer strikingly weakened.

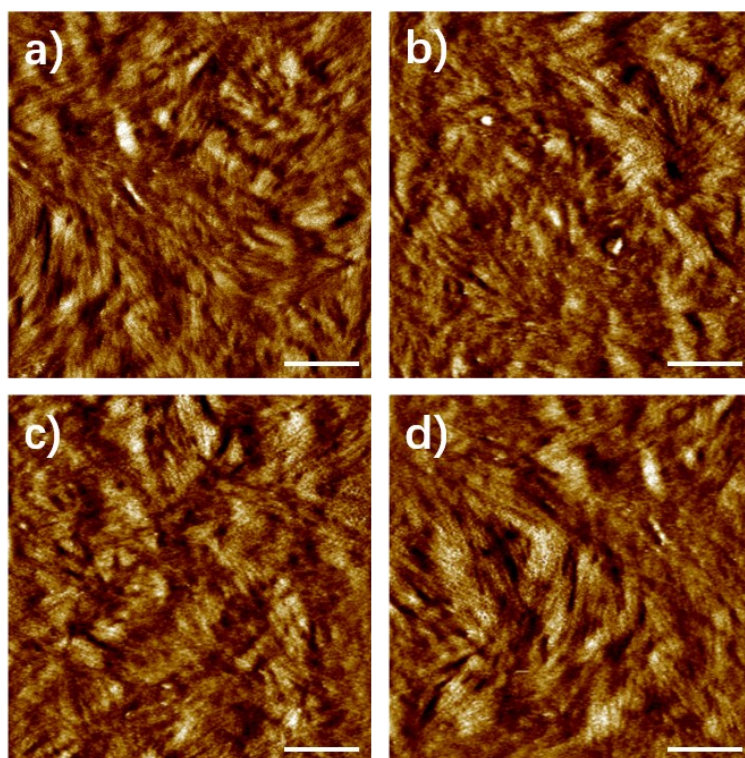


Figure S3 AFM phase images of supramolecular polymer **6** ~ **9** from **a** to **d**. All the polymer showed the nano-fiber structures. Scale bar is 200 nm.

The supramolecular polymers with the same chemical structure but different molecule weight telechelic polymers were prepared to investigate the effect of the different contents of the UPy moieties on the viscoelastic properties. The same UPy structure with the methyl at six-position as the end group and polybutadiene with different molecule weight as the telechelic polymer backbone were employed to obtain the tough supramolecular polymers. It was designed in this series polymer that the different molecular weight telechelic polymer will cause the change of the content of the UPy moiety therefore affect the degree of the microphase separation which could affect the properties of the supramolecular polymer distinctly.

Polymer **6** to **9** exhibited a distinct, well defined nano-fibers structure in figure S3,

indicating that the supramolecular polymer **6** ~ **9**, where the methyl is at six-position, had obvious phase separation, which could also be verified by the differential scanning calorimetry. Figure S3b to figure S3d showed the AFM image of supramolecular polymer **7** ~ **9** and the amount of the nano-fiber structure decreased gradually, which is in agreement with the change of the contents of the UPy moieties. FT-IR and ¹H-NMR spectra (ESI) indicated that the UPy moiety formed into quadruple hydrogen bonding system both in synthon and in polymer (solid film and in chloroform).

SAXS patterns

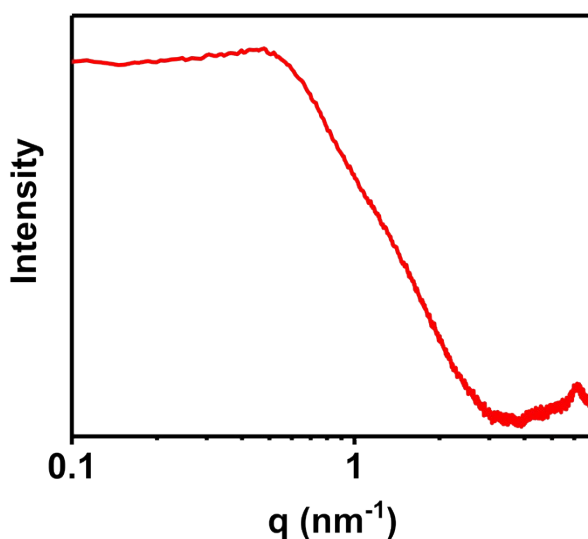


Figure S4 The SAXS pattern of polymer **6**.

The SAXS pattern of polymer **6** was shown in figure S4. As illustrated, with the little steric hindrance UPy moieties, the supramolecular showed a distinct scattering peak at q value about 6 nm^{-1} . Combined with the phase image of the AFM tests, it could be identified that the microphase separation occurred both on the surface and the inner of the solid.

DSC curves

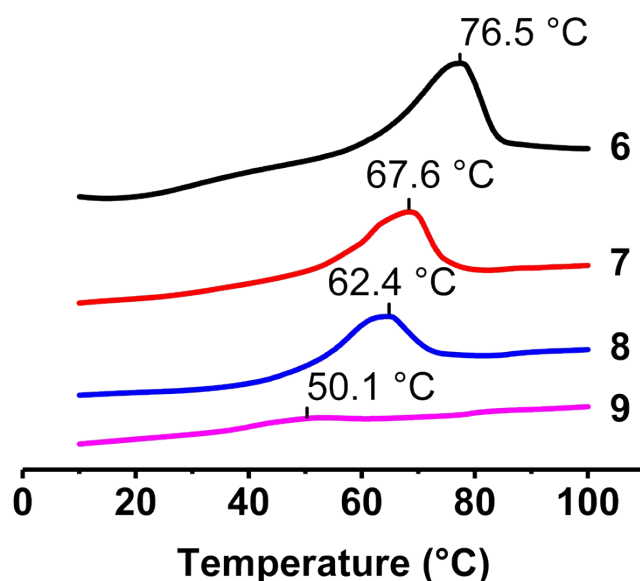


Figure S5 The DSC curves of polymer 6 ~ 9 (endo up). First heating run, 20 K/min, curves are shifted vertically for clarity. The melting point decreased with the contents of the UPy moieties decreased. Polymer 6 has a highest constant pressure melting enthalpy (9.40 J/g), while the polymer 7 came the second (6.74 J/g). A very faint melting peak was observed of polymer 9. The melting point and the melting enthalpy fitted the content of the UPy moieties linearly. (Figure S6a, b)

The AFM images could demonstrate the intuitionistic phase-separation motif of the UPy stacks, while the differential scanning calorimetry (DSC) could measure the degree of phase-separation quantitatively. The decrease of the amount of nano-fiber structures indicated that the degree of micro-phase separation is reducing. The DSC test confirmed the assumption. The melting of the UPy nano-fiber in the heating process was recorded by DSC tests and the enthalpy-change of the melting peak was calculated. The thermal and mechanical properties of polymers 6 ~ 9 were listed in table S3. As shown in table S3, polymer 6 has a highest constant pressure melting enthalpy (9.40 J/g), while the polymer 7 came the second (6.74 J/g). A very faint melting peak was observed of polymer 9. Because of the difference of the molecule weight in backbone of the polymer, the T_g was affected by the telechelic polybutylene significantly. With the molecule weight increased, the T_g moved to the lower temperature. The ΔEnthalpy

versus the UPy content calculated according to the molecule weight was plotted in figure S6a. As expected, the enthalpy changes of the melting peak fitted the content of UPy moiety linearly, meaning that the melting enthalpy could represent the amount of the UPy stack nano-fiber formed in the supramolecular polymer and the degree of the micro-phase separation. Moreover, in table S3, it was clearly demonstrated that the T_m fell dramatically with the reducing of UPy contents, indicating that the content of the nano-fibers in the polymer decreased by degrees. (figure S6b) Because the supramolecular polymer has the similar chemical structure, these distinct changes should only be induced by the different contents of the nano-fibers structure formed by the UPy moiety.

Table S3 Molecular weight and thermal properties of supramolecular polymers **6 ~ 9**.

Polymer	Content of UPy moiety	M_n (g·mol ⁻¹)	T_g (°C)	T_m (°C)	melting enthalpy (J·g ⁻¹)	peak area (Mpa·min)
6	0.23598	2486	-65.8	76.5	9.40	1297
7	0.20327	2886	-69.2	67.6	6.74	1227
8	0.18236	3217	-69.8	62.4	5.22	1190
9	0.12792	4586	-72.5	50.1	0.54	1067

In order to characterize the effect of different contents the UPy end groups on the viscoelastic properties, the static tension tests and dynamic mechanical analysis (DMA) was performed. (Figure S9, S10 and S11) The elasticity modulus represents the elastic properties of the materials, which could be enhance by the UPy dimer stack nano-fibers hard-segment, increased with the UPy content exponentially. (Figure S6c) The loss modulus represented the viscosity properties and the energy lost in the vibration process of the material, which could be affected by series ingredients such as the length of the

polymer chains, the viscosity of the polymer chain, the interaction between the polymer chains and so on. In order to determine the influence of UPy stack induced internal friction on the loss modulus in the whole process of the glass transition, based on the above assumptions, the areas of the loss modulus peak between -60 °C to 20 °C were calculated and exhibited in figure S6d. Interesting result was discovered that the calculated peak area of loss modulus increased linearly to UPy content. The peak area of the loss modulus could represent the total energy dispersed in the test process. With the content of UPy hard-segment increased, there was more energy dissipated from the internal-friction raised from the interaction of the UPy nano-fibers at the glass transition period.

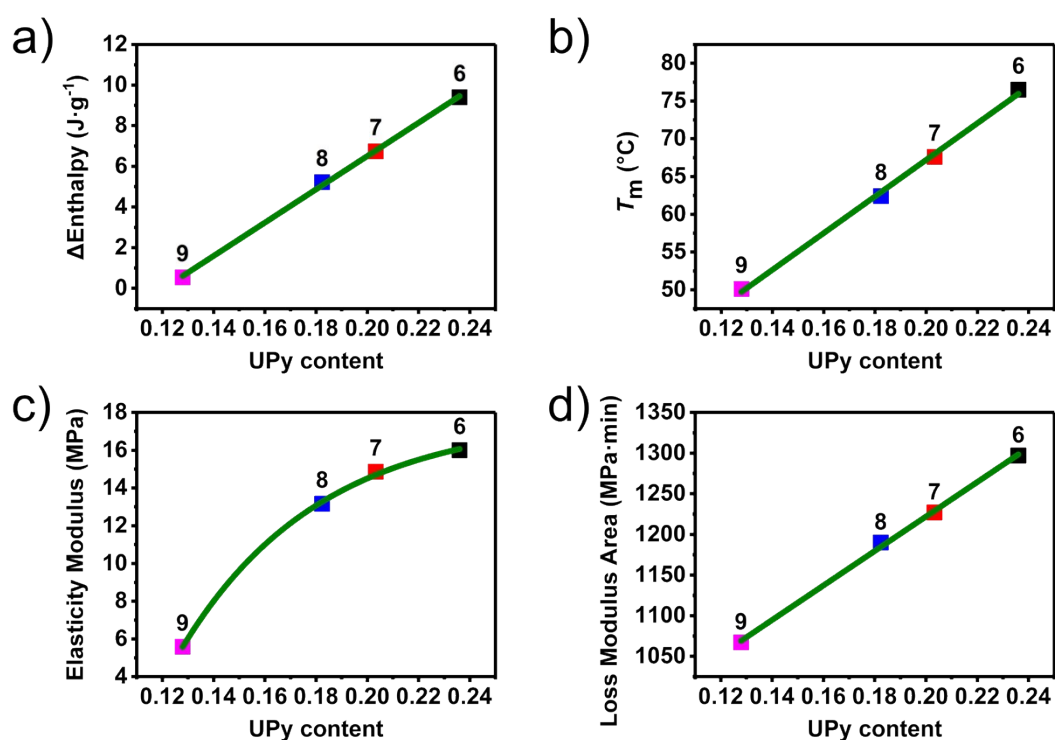


Figure S6 a) The enthalpy changes of the melting peak, b) the T_m , c) the elasticity modulus and d) the peak areas of loss modulus polymer 6 ~ 9 were plotted and fitted. The black dot is the origin data and the red line is the fitted curve.

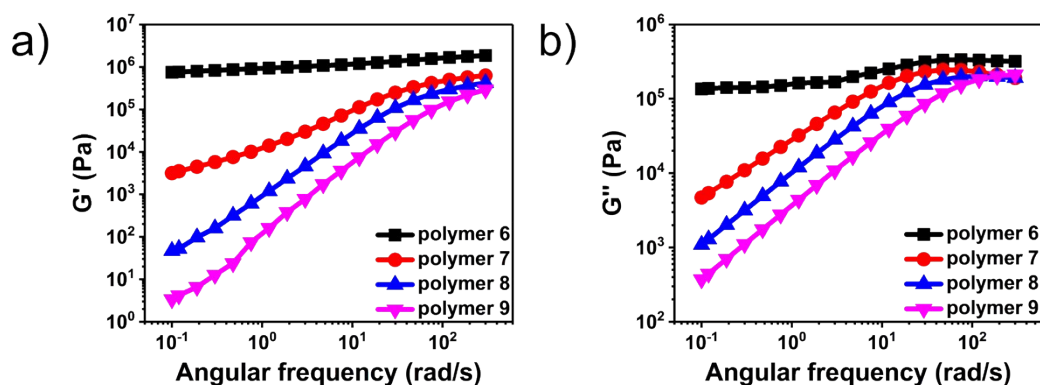


Figure S7 The rheology test of the supramolecular polymer **6** to **9**.

The small amplitude oscillatory shear tests, that is, frequency sweep, were carried out in the linear viscoelastic region. Figure S7 showed the storage modulus and loss modulus against angular frequency for the different supramolecular polymer samples. Be similar to polymer **1** and **2**, a plateau in the storage modulus could be observed of polymer **6** and polymer **7**, which was caused by the reversibility of the association of the quadruple hydrogen bonding units. However, the presence of a plateau can also be an indication that small clusters of hydrogen-bonded units are present. These clusters act as hard domains and physical crosslinks in supramolecular polymers, which corresponding to the nano-fibers structures in the solid. As shown in figure S7, both storage modulus and loss modulus enhanced with the increasing of the degree of microphase separation, which is agreed with the result of the dynamic mechanical analysis tests.

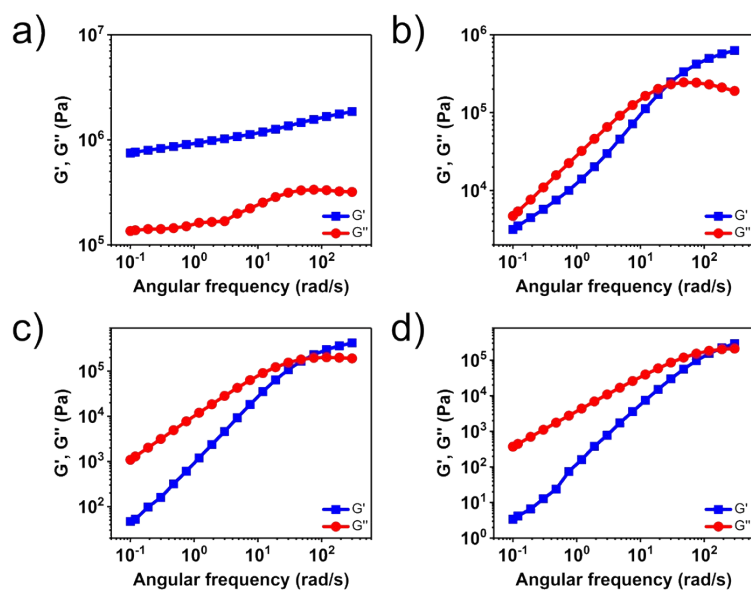


Figure S8 The rheology tests of sample 6 to 9 from a to d.

Be similar to polymer 1 to 5, polymer 6 to 9 showed a change of the slope ratio from 1:1 to 1:2, indication that the interaction between the UPy dimmer weakened with decrease of the contents of the UPy moieties.

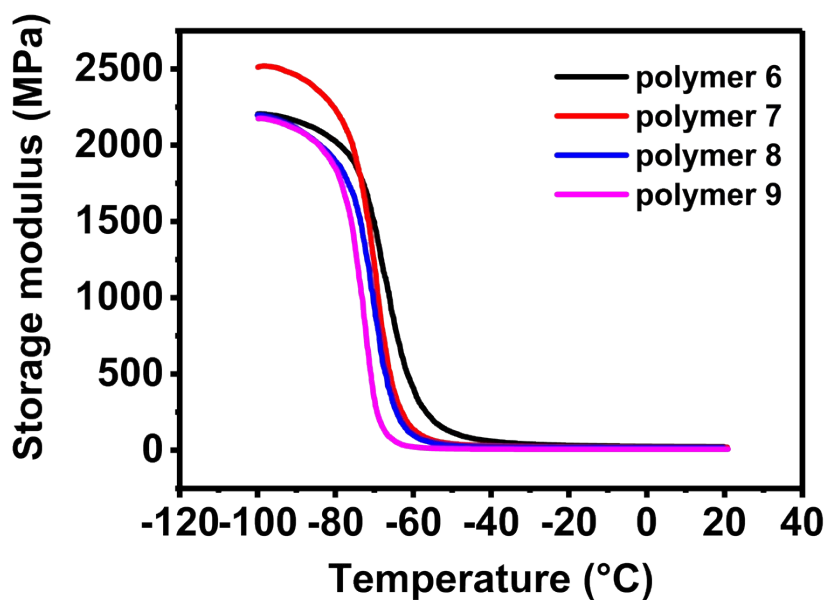


Figure S9 The storage modulus of polymer 6 ~ 9.

With the increase of the content of the UPy moieties, the length of the molecular chain, and the molecular weight, decreased simultaneously. The storage modulus is affected

by the hard-soft segment phase-separation and the interaction of the polymer chains. The interaction of the polymer chain was affected by the molecular chain and the longer polymer chains is, there are more entanglement of the polymer chains. Combined with the contrary influence, supramolecular polymer 6 ~ 9 showed almost the same storage modulus.

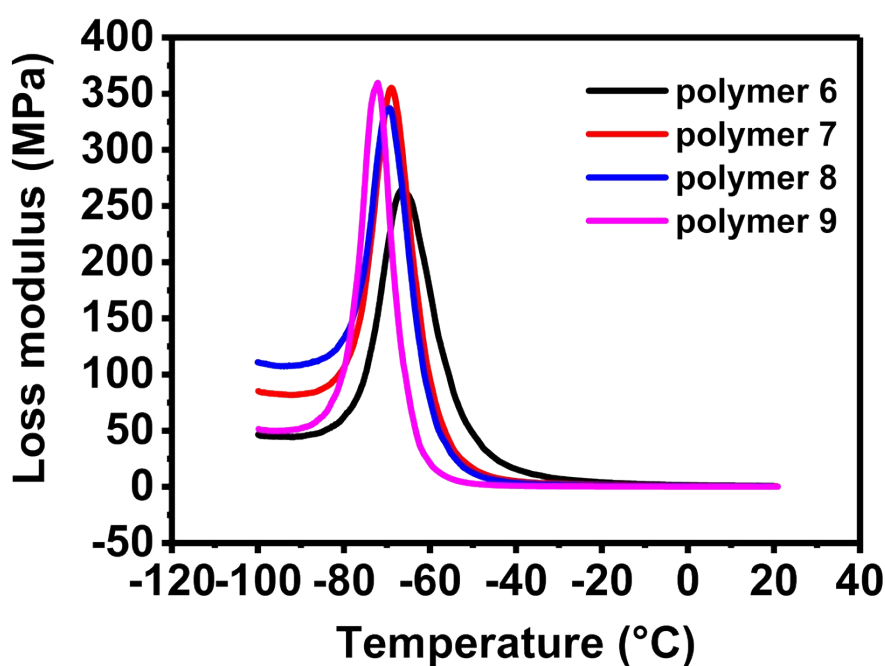


Figure S10 The loss modulus of polymer 6 ~ 9.

The loss modulus represents the energy dissipated in the test progress. At the glass transition temperature, the UPy moieties still bonded via the quadruple hydrogen bonding and the nano-fiber structures were still exist. The peak of the loss modulus was mainly influenced by the telechelic polymer. While in the entire tests process, the strong bonded UPy moieties gradually weaken with the temperature increased and the internal friction induced by the reptation and relative slide could dissipate more energy. It could be seen in figure S6 that with the increase of the content of UPy moieties, the peak gradually broadened and the areas of the loss modulus increased linearly. (figure S6d)

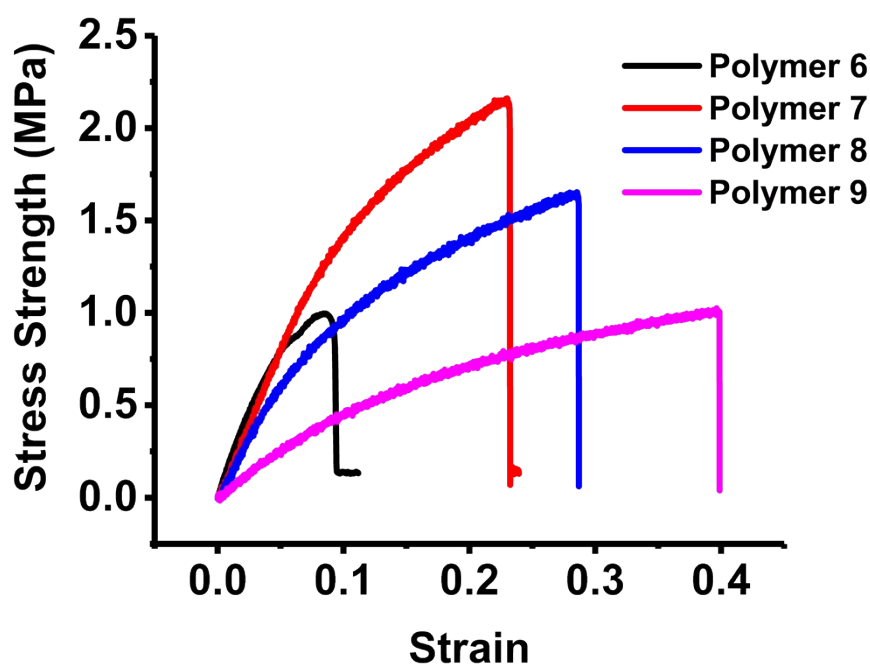


Figure S11 The static tension tests curves of polymer 6 to 9.

The UPy moieties act as the hard-segment in the polymer and it would enhance both the modulus and the fracture strength. But because of the excessive amount of the UPy structure in polymer 6, it showed a semi-crystal solid and was fragile. It was very easy to be broken in the test hence the polymer 6 showed the minimum fracture strength. The elastic modulus showed an increasement with the content from polymer 6 to polymer 9. The telechelic polymer act as the soft-segment which would improve the elasticity. With the contents of the UPy moieties decrease, meaning the content of the polymer butylene increase, the elongation of the polymer increased from polymer 6 to polymer 9.